Influence of back barrier layer thickness on device performance of AlGaN/GaN MOS-HEMT

Aboo Bakar Khan[1]*, Mohini Sharma[2], Syed Gulraze Anjum[1] and Mohd Jawaid Siddiqui[1]

[1]*Department of Electronics Engineering, Z H College of Engineering & Technology AMU, Aligarh 202002, UP, India*
[2]*Department of Electronics Engineering, Banasthali University, Tonk, Rajasthan 304022, India*

*Corresponding author

DOI: 10.5185/amp.2018/7000
www.vbripress.com/amp

Abstract

In this work, we have performed the influence of back barrier layer thickness variation on AlGaN/GaN Metal Oxide Semiconductor High Electron Mobility Transistor (MOS-HEMT) device with 0.5 µm Schottky gate length. The AlGaN back barrier layer presented increases the conduction band with respect to GaN channel layer so that more no of electron confinement into the GaN channel layer and improve the high-frequency performance. The effect of the back-barrier layer thickness is performed by using 2-D TCAD Atlas Silvaco numerical simulation tool by taking Hydrodynamic mobility model. Due to a large amount of two-dimensional electron gas (2-DEG) density at the AlGaN/GaN heterointerface of the MOS-HEMT device higher drain current density is obtained. The 2-D simulation is carried out with a variation of back barrier layer thickness for various device parameter such as transfer characteristics (I_d-V_g), drain current with a drain voltage (I_d-V_d), transconductance (g_m), drain induced barrier lowering (DIBL), conduction band energy and electron concentration into the channel. In this simulation, we have also performed the RF performance like a gate to source capacitance (C_{gs}) and current gain cut-off frequency of AlGaN/GaN MOS-HEMT device. The results obtained by variation of AlGaN back barrier layer thickness can be a better solution in future analog and RF device application. Copyright © 2018 VBRI Press.

Keywords: MOS-HEMT, 2-DEG, transconductance, cutoff frequency.

Introduction

The AlGaN/ GaN heterostructure based HEMT has been highly developed from two decades and set up many applications in various areas of advanced microelectronics. Typically, AlGaN/ GaN-based heterostructure use in high electron mobility transistors (HEMTs) and metal oxide semiconductor high electron mobility transistors (MOS-HEMTs) for high-power and high-frequency devices **[1-3]**, also in various fields like in biological sensors and chemical **[4-6]**. Recently AlGaN/ GaN base heterostructure are used in piezo electronics **[7, 8]**. The use of gate oxide in HEMTs **[9,10]** an additional advantage of MOS-HEMT structures have been suppressing subthreshold leakage current and surrounding punch through phenomenon **[11]**.

GaN material with wide band gap energy, high thermal conductivity, and high saturation drift velocity is preferred material for the development of high-temperature, high- frequency, and high-power switching devices **[12-14]**. Important progress has been made with improvements in the material quality, device fabrication, and the epitaxial layer designs **[15]**. Al_xGa_{1-x} N/GaN high electron mobility transistors(HEMTs)realized from III-N semiconductor materials with wide band gaps are currently the most promising contenders for power microwave applications. HEMTs based on AlGaN/GaN give sufficiently promising results to carry out small-scale mass production for very specific applications. They are used in military applications such as radar systems, satellites, and wireless communications. GaN-based high electron mobility transistors (HEMTs) have now been established as a main focal point for high frequency and power switching and amplification.

In this paper, the 2D simulations are performed on proposed AlGaN/GaN DG MOS-HEMT device by taking into account high-frequency application. We have performed the effect of back barrier layer thickness of 1nm, 2nm, 5nm and 10nm gate length AlGaN/GaN MOS-HEMT device structure. In this simulation, various important device parameters such as transfer characteristics, transconductance, frequency, capacitance, electric field strength and DIBL, and have been done with a different back barrier layer thickness (d_{bb}). We have also performed RF analysis to analyze the important figure of merits (FOMs) like f_T, g_m and gate capacitance with a variation of d_b. The aim of the simulation of this device for achieving high ON-state current and better performance of the device. The device structure details such as doping concentration and its dimension are provided in Section 2. The simulation model of this device has been discussed in Section 3. The simulation results have been discussed in Section 4, followed by conclusion discussed in Section 5.

Device description

In this paper AlGaN/GaN HEMTs 2D structure have been studied, the layered structure is indicated in **Fig. 1**, can produce by metal organic chemical vapor deposition (MOCVD) or by molecular beam epitaxy (MBE) and chemical beam epitaxy (CBE) on a sapphire substrate. The Schottky barrier layer of 12 nm is used in this structure which is having wider band gap with respect to the channel layer. Because of more bandgap discontinuity at the AlGaN/GaN heterointerface, where the unrestricted electron diffuses into GaN channel layer from AlGaN doping layer and it forms 2 DEG (two-dimensional electron gas), which allows high sheet charge density and recovers the carrier confinement in the channel. There is a small gap from gate metal to the channel layer because of thinner AlGaN Schottky layer and because of this it results in higher transconductance but decreases the breakdown voltage of the device. The device have 1 nm AlGaN spacer layer, 20 nm GaN channel layer, and sapphire substrate. In this work, a back-barrier layer of different thickness is used. Hence, we simulate the result at thickness 1 nm, 2 nm, 5 nm, and 10 nm. The 2-DEG formation in the channel is controlled by a Schottky gate, which is 100 µm wide and 0.5 µm long. Source and drain width is 1 µm long and doped with a donor concentration of 10^{21} cm^{-3} extended down to the GaN channel. In **Table 1**, indicates the physical properties of wide bandgap $Al_{0.3}Ga_{0.7}N$ and narrow bandgap GaN. The model is used for simulation of purpose MOS-HEMT structure is described in the next section.

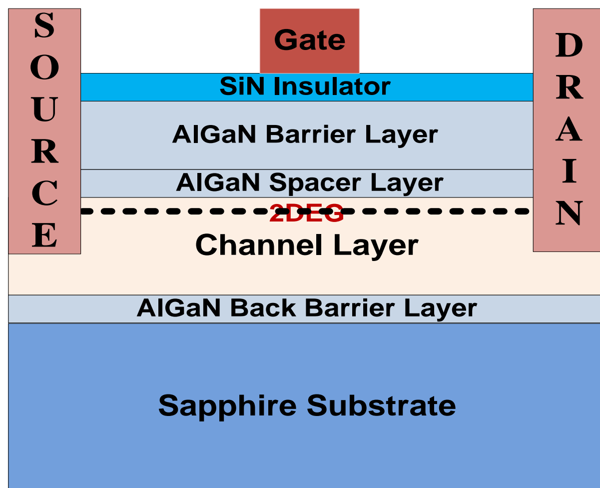

Fig. 1. The layered structure of AlGaN/GaN MOS-HEMT device.

Simulation model description

In this section, **Fig. 1** shows the simulated AlGaN/GaN MOS-HEMT device structure. Furthermore, the AlGaN/GaN HEMT device structure is simulated and it compared the performance of the AlGaN/GaN MOS-HEMT device. The 2D simulation has been done by using TCAD Atlas numerical simulation tool **[16]**. Atlas numerical tool has numerous types model which can be used for simulation. In this simulation, Hydrodynamic mobility model has been taken into account for device simulation. For non-equilibrium condition, this model generally used like quasi-ballistic transport phenomenon. Various imperative physical impacts are taken account to the simulation like effective mass variability, narrowing of the band gap, doping dependent mobility, polarizations and spontaneous. For recombination, SRH is used with Shockley-Read-Hall the value of auger recombination are t_{SRH} = 60 ns, $C_{auger} = 4x10^{29}$ cm^6/s and $C_{ard} = 1.4x10^{-9}$ cm^3/s **[17]**.

Hydrodynamic mobility model explains Poisson and continuity equations as below:

$$\nabla.\varepsilon\nabla\phi = -q(p - n + N_D - N_A) - \rho_{trap} \quad (1)$$

$$J_n = q\mu_n(n\nabla E_c + kT_n\nabla_n + kn\nabla T_n - 1.5nkT_n\nabla ln m_n \quad (2)$$

where ε indicate the permittivity, ϕ denote electrostatic potential, electron charge is represented by q, p and n suggest for hole and electron densities respectively, N_D and N_A symbolise the concentration of ionized donors and accepters respectively and ρ_{trap} denote total charge density which is contributed by fixed charges and traps, E_c represent conduction band energy, T_n for electron temperature and effective mass of electron represented by m_n. From the equation (Hydrodynamic mobility model) it finds that electron mobility is not only the function of doping but also it depends on field is given by **[18]**.

$$\mu_{n,dop} = \mu_{min} + \frac{\mu_d}{1+(N_{dop}/N_0)^A} \quad (3)$$

$$\mu_{n,field} = \frac{\mu_{no}+(\frac{v_{sat}}{E_0})(\frac{F}{E_0})^4}{1+(F/E_0)^4} \quad (4)$$

$$\frac{1}{\mu_n} = \frac{1}{\mu_{n,dop}} + \frac{1}{\mu_{n,field}} - \frac{1}{\mu_{no}} \quad (5)$$

$$\mu_{min} = A_{min}\left(\frac{T}{300}\right)^{\alpha_m} \qquad \mu_d = A_d\left(\frac{T}{300}\right)^{\alpha_d} \quad (6)$$

$$N_0 = A_N\left(\frac{T}{300}\right)^{\alpha_N} \qquad A = A_a\left(\frac{T}{300}\right)^{a} \quad (7)$$

where, $\mu_{n,field}$ denotes the field dependent mobility at low doping, μ_{n0} denote low field mobility at low doping, $\mu_{n,dop}$ is signify mobility due to impurity scattering, F and N_{dop} denoted by driving force and doping concentration respectively. For the simulation, the important parameter which are take $v_{sat} = 1.3 \times 10^7 cm/s$; E_0=1.5× $10^5 V/cm$ and μ_{min}=800cm^2/V-s. μ_d, N_0 and A are the essential temperature dependent constraint.

Table 1. Physical properties of AlGaN and GaN [19, 20].

Material	$Al_{0.3}Ga_{0.7}N$	GaN
E_g (eV)	3.96	3.4
CBO (eV)	……..	0.31
VBO (eV)	……...	0.39
E_o	9.5	9.5
Lattice Constant (A)	3.19	3.186
μ_e (cm^2/Vs)	600	1160
μ_p (cm^2/Vs)	10	22

Copyright © 2018 VBRI Press

Results and discussion

Fig. 2 indicates the diagram of the energy band of AlGaN/GaN MOS-HEMT heterostructures and it also shows the formation of the 2-DEG at the heterointerface of AlGaN/GaN due to band gap energy differences. From the simulation, the result shows that a very high electron concentration is found at the AlGaN and GaN interface in MOS-HEMT. Because oxide provides work as a large energy barrier. The results display that the electron transfer from higher band gap material AlGaN into low band gap material GaN and form 2DEG. A small amount (negligible) of electron concentration is found across donor layer because it is highly doped.

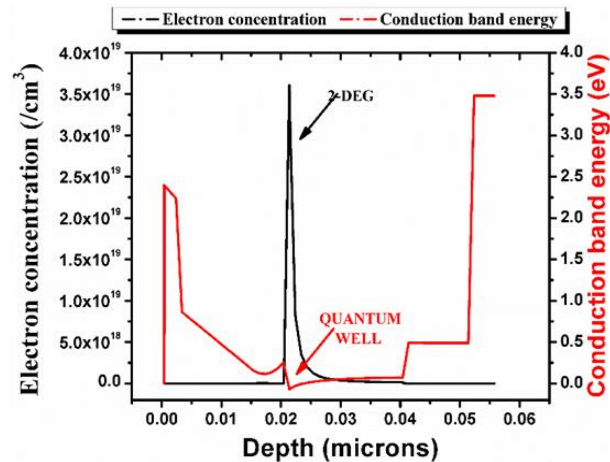

Fig. 2. Conduction Band Energy with Carrier Concentration of MOS-HEMT.

High electron concentration is provided due to high carrier current densities. The transfer characteristics of MOS-HEMT are shown in **Fig 3**. Due to extra-large back barrier height, it increases the drain current of the MOS-HEMT device. The back barrier layer thickness plays a vital role in device performance. The sheet charge density in the channel increases due to the thicker barrier layer and keep away channel electron from the HfO_2/AlGaN interface. The transfer characteristics of MOS-HEMT with back barrier layer thickness variation are shown in **Fig 3**.

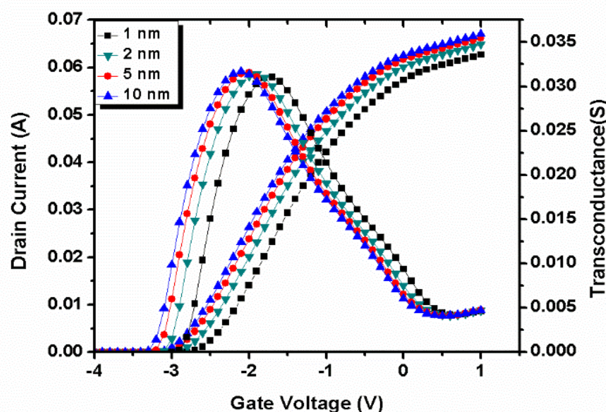

Fig. 3. Transfer characteristics and Transconductance with gate voltage of AlGaN/GaN MOS-HEMT device structure at different barrier layer thickness V_{ds} = 1V.

The result shows as back barrier layer thickness increases; it increases the drain current of the MOS-HEMT. In this, the result is simulated at different back barrier layer i.e. 1 nm, 2 nm, 5 nm and 10 nm. At 10 nm, the higher drain current is observed and shift towards the more negative side. It is observed that the 2-DEG carrier concentration increases with back barrier layer thickness in the channel of heterostructure HEMT. **Fig. 3** also indicates the variation in transconductance with a gate voltage of AlGaN/GaN MOS-HEMT. We varied back barrier layer at different thickness i.e. 1 nm, 2nm, 5nm and 10 nm. The peak of transconductance curve for back barrier layer with a higher thickness is high. The simulation result shows that the transconductance of 10 nm in MOS-HEMT is high. In MOS-HEMT device the threshold voltage goes to more negative side due to which low transconductance peak is observed.

The variation of electric field position throughout channel from gate to substrate is shown in **Fig. 5.** From the simulation, it is found that the electric field of MOS-HEMT device is increased. Due to Si_3N_4 dielectric layer, more electron confinement into the channel at AlGaN/GaN interface in MOS-HEMT device as compared to HEMT device results in the high electric field in MOS-HEMT device.

Fig. 4 represents the difference of electric field with back barrier layer thickness throughout the channel from the front gate to back gate. As the back barrier layer thickness decreases, the distance between the channel and gate decreases because of which the induced electric field is higher in the device. The electric field is measured with different thickness of back barrier layers. We found highest back barrier layer at 10nm. The high electric field, cause higher depletion or in another hand low electron concentration in the channel (2DEG). Low 2DEG cause low drain current.

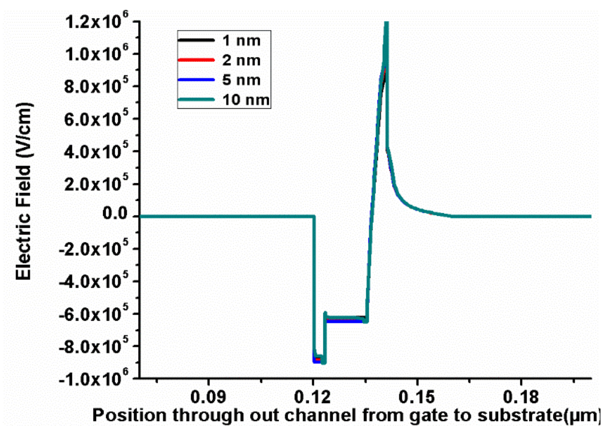

Fig. 4. Variation of Electric field of AlGaN/GaN MOS-HEMT structure at different back barrier layer thickness(db).

The variation of gate capacitance with gate voltage at high frequency (1 MHz) of HEMT device is shown in **Fig. 5**. From the simulation results, it is found that the gate capacitance of MOS-HEMT is decreased as compared to HEMT device. The gate capacitance of MOS-HEMT can be expressed as **[21]**:

$$\frac{1}{C_{gs}} = \frac{1}{C_{ox}} + \frac{1}{C_{Barrier}} \quad (8)$$

where, $C_{Barrier}$ AlGaN depleted barrier layer capacitance and C_{ox} represents the gate oxide capacitance.

The RF operation of HEMT and MOS-HEMT device is performed, taking small signal radio frequency figure of merit such as cut-off frequency f_T. f_T play an important role in high speed digital system in the form of speed and high swing. The cut off frequency f_T of current gain is well-defined as the frequency at which current gain of a two-port network goes to unity. It is the maximum frequency till the device can work for current amplification. Under the assumption that feedback capacitance is negligible in HEMTs, f_T is given by:

$$f_T = \frac{g_m}{2\pi C_{gs}} = \frac{v_{sat}}{2\pi L_g} \quad (9)$$

where, C_{gs} denotes gate to source capacitance, v_{sat} denotes saturation carrier velocity in the channel and L_g denotes gate length of the device. The equation eqn-12 shows that improving saturation velocity and down-scaling gate length are the basic approaches to increase f_T [**22**].

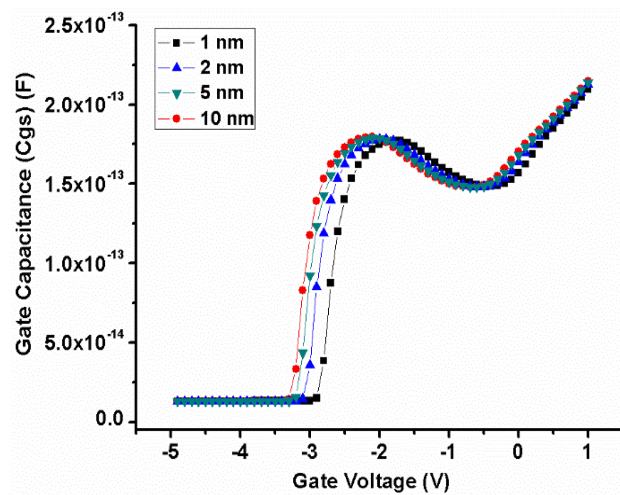

Fig. 5. The variation of Gate Capacitance with Gate Voltage MOS-HEMT device at different back barrier layers.

Fig. 6 indicates the variation of f_T with gate voltage at different back barrier layer thickness, demonstrating an increase in cut-off frequency with reduction of back barrier layer thickness. Initially cut-off frequency f_T starts to rise with gate voltage and then drops gradually. Due to feeble inversion at the initially f_T is increasing with g_m and comparatively stable C_{gs}. Further as gate voltage increases, C_{gs} increase accelerated due to this f_T decreases and g_m decreases. The maximum value of f_T occurs at the point someplace among the lowest C_{gs} and peak of g_m. As the barrier layer thickness decreases, f_T upsurges because the growing rate of g_m with decline barrier layer thickness is higher (**Fig. 4**), then the increasing amount of C_{gs} (**Fig. 6**). Thus, considering the maximum cut-off frequency achieved AlGaN/GaN DG MOS-HEMT, which can be promising to potential candidature to design for high frequency application.

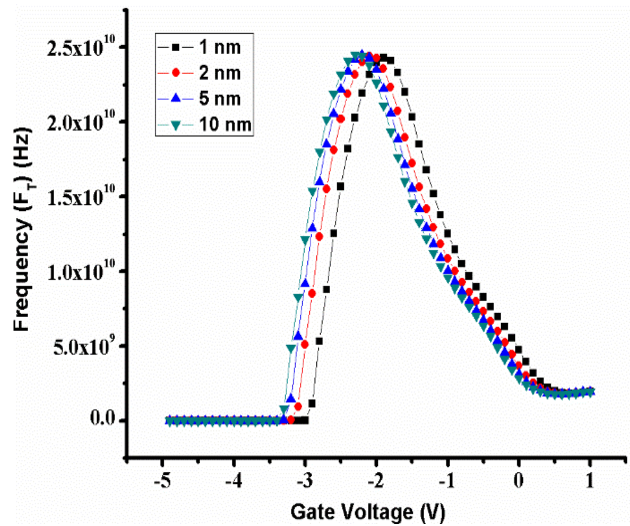

Fig. 6. Variation of the Cutoff frequency with Gate Voltage at different barrier layer thickness d_b at V_{ds} = 1V.

Conclusion

In this research paper, we have explored the performance of AlGaN/GaN MOS-HEMT device with respect to AlGaN back barrier layer. The device with back barrier exhibited pretty decent performance. One good DC feature of the back-barrier device is smaller drain-induced barrier lowering (DIBL) at shorter gate lengths due to the smaller output conductance. We have simulated all the parameters like I_d-V_g, transconductance, frequency, capacitance, electric field and DIBL at different thickness of back barrier layer i.e. 1nm, 2nm, 5 nm and 10 nm. At different thickness, variations are visible for all parameters. At 10nm, we found better results than at any other value. The confinement of the 2DEG in the channel is enhanced and short channels effects mitigated to certain extends. Thus, use of AlGaN back barrier in such devices can be effectively deployed to scale the gate length of the device and attractive for future analog and high-frequency RF applications. However, the optimization of back barrier layer along with gate length to operate the device in normally-off mode is left for the future scope.

Acknowledgements

Authors are highly grateful to Research Laboratory of Electronics Engineering Department, AMU, Aligarh, India under DSA-I scheme supported by UGC-SAP program. Authors are also thankful to TEQIP -II scheme for providing financial support in completing this research work.

References

1. Shen, L.; Heikman, S.; Moran, B.; Coffie, R.; Zhang, N.; Buttari, D.; Smorchkova, L. P.; Keller, S.; DenBaars, S. P.; Mishra, U. K. IEEE Electr. Device Lett. **2001**, 22, 457.
2. Mishra, U. K.; Shen, L.; Kazior, T. E.; Wu, Y. F. Proc. IEEE **2008**, *96*, 287.

Copyright © 2018 VBRI Press

3. Chung, J. W.; Hoke, W. E.; Chumbes, E. M.; Palacios, T. IEEE Electr. Device Lett. **2010,** *31,* 195.
4. Schalwig, J.; Müller, G.; Eickhoff, M.; Ambacher, O.; Stutzmann, M. Sens. Actuat. B Chem. **2002,** *87,* 425.
5. Kang, B. S.; Kim, S.; Ren, F.; Johnson, J. W.; Therrien, R. J.; Rajagopal, P.; Roberts, J. C.; Piner, E. L.; Linthicum, K. J.; Chu, S. N. G.; Baik, K.; Gila, B. P.; Abernathy, C. R.; Pearton, S. J. Appl. Phys. Lett. **2004,** *85,* 2962.
6. Kang, B. S.; Wang, H. T.; Ren, F.; Pearton, S. J. J. Appl. Phys. **2008,** *104,* 031101.
7. Kristian Berland, Superlattices and Microstructures. **2011,** *50,* 411.
8. Zimmermann, T.; Neuburger, M.; Benkart, P.; Hernandez-Guillen, F. J.; Pietzka, C.; Kunze, M.; Daumiller, I.; Dadgar, A.; Krost, A.; Kohn, E. IEEE Electr. Device Lett. **2006,** *27,* 309.
9. Qi, Z.; Hongwei, C.; Chunhua, Z.; Feng, Z. H.; Cai, S. J.; Chen, K. J. IEEE Electron Device Lett. **2012,** *33,* 38.
10. Khan, M. A.; Hu, X.; Sumin, G.; Lunev, A.; Yang, J.; Gaska, R.; Shur, M. S. IEEE Electron Device Lett. **2000,** *21,* 63.
11. Treidel, B.; Brunner, E.; Hilt, F.; Cho, O.; Würfl, E.; Trankle, J. Electron Devices, IEEE Trans. **2010,** 57, *11,* 3050.
12. Shur, M. S.; Gaska, R.;Khan, A.; Simin, G. Fourth IEEE International Caracas Conference on Devices, Circuits and Systems, Aruba, **2002**, 17.
DOI: 10.1109/ICCDCS.2002.1004074
13. Vetury R.; Zhang, N. Q.; Keller, S.; Mishra, U. K. IEEE Transactions on Electron Devices, **2001,** *48, 3,* 560.
DOI: 10.1109/16.906451
14. Wells, A. M.; Uren, M. J.; Balmer, R. S.; Hilton, K. P.; Martin, T.; Missous, M. Solid-state electronics, **2005**, *49, 2,* 279.
15. Mishra, U. K.; Shen, L.; Kazior, T. E.; Wu, Y. F.; Proc. IEEE. **2008**, *96,* 287.
16. Silvaco. TCAD Atlas device user's manual August 26, **2016**.
17. Ji, G.; Liu, H. G.; Su, Y. B.; Xiong, C. Y.; Zhi, J. Chin. Phys. B. **2012**, *21,* 058501.
18. Khan, A. B.; Siddiqui, M. J.; Singh, M. M.; Thaseena, C. K. IEEE International Conference in Multimedia, Signal Processing and Communication Technologies (IMPACT), **2013,** 264.
19. Swain, S. K.; Adak, S.; Pati, S. K.; Sarkar, C. K. Superlattices and Microstructures **2016,** *97,* 258.
20. Higashiwaki, M.; Matsui, T. Japan Journal of Applied Physics **2004,** *43*, 147.
21. Vitanov, S.; Palankovski, V.; Maroldt, S.; Quay, R. Solid-State Electronics **2010**, *54,* 1105.
22. Sun, X.; Saadat, O. I.; Chang-Liao, K. S.; Palacios, T.; Cui, S.; Ma, T. P. Appl. Phys. Lett. **2013,** *102*, 10.

Copyright © 2018 VBRI Press